Shap. Mem. Superelasticity (2015) 1:78–84
DOI 10.1007/s40830-015-0006-3

Advanced Electron Microscopy Characterisation of Important Precipitation and Ordering Phenomena in Shape Memory Systems

Dominique Schryvers[1]

Published online: 21 April 2015

Abstract The present paper discusses some important aspects of precipitation and ordering in alloy systems that show a martensitic transformation and can or are used as shape memory or superelastic metallic systems. The precipitates are investigated by a variety of conventional and advanced electron microscopy techniques, including atomic resolution, 3D slice-and-view, energy loss spectroscopy etc. Depending on the system, such secondary phases can decrease the probability of a displacive transformation by changing the phase stability in the system, such as in the case of Ni–Al or Ni–Ti–Pd, or can mechanically hinder the passage of the transformation interface, as in Ni–Ti–Nb. On the other hand, properly controlling the nucleation and growth of some precipitates can strongly improve the properties of some types of materials, as is the case for the well-known Ni_4Ti_3 precipitates.

Keywords Precipitation · Ordering · TEM · SEM · Ni–Al · Ni–Ti

Introduction

The appearance of shape memory (SM) and superelasticity (SE) behaviour in selected alloys is based on the diffusionless and reversible martensitic phase transformation. According to the classification scheme first presented by Cohen et al. [1], this type of transformation implies a homogeneous lattice-distortive strain (as apposed to shuffle movements), which transforms one Bravais lattice into another one. Moreover, the strain needs to be shear dominated (as opposed to dominated by dilatations) so that an undistorted line exists between the parent and product phase. For a genuine martensitic transformation, the kinetics and morphology also need to be dominated by the strain energy (as opposed to being due to atom vibrational displacements). Typical examples of alloys accommodating this type of transformation are low-carbon steel, some Cu-based alloys and Ni–Ti-based systems (although many other systems exist as well). However, for alloys to perform properly in the functional circumstances of shape memory and superelasticity as required by the conditions of a particular application, the system needs to be trained under well-defined thermal and mechanical conditions. As a result of this training (and especially its thermal component), the micro- and sometimes also the nanostructure of the alloy can become very complex, often including the precipitation of (meta)stable secondary phases in the form of precipitates, ordered structures etc. Without these particular structural features, the requested shape memory and superelastic behaviour would often not occur (or at least not to the satisfaction of the user), but since they are also often more stable than the metastable martensite phase, they can overrule the displacive martensitic transformation so the competition and interactions between the different structures need to be understood very well.

In the present paper, the focus will be on the use of advanced scanning and transmission electron microscopy (S/TEM) techniques used for the characterisation of such micro- and nanostructures. For a first example we return to conventional high-resolution TEM (HRTEM) and to the Ni–Al system, an alloy was heavily investigated in the second half of the previous century to understand the

✉ Dominique Schryvers
nick.schryvers@uantwerpen.be

[1] EMAT, University of Antwerp, Groenenborgerlaan 171, 2020 Antwerp, Belgium

physical properties and driving forces of the (pre-)-martensitic transformation. In the second example, various more advanced S/TEM examples aiming for better quantification of the all important but metastable Ni_4Ti_3 precipitates in near-equiatomic Ni–Ti will be discussed. For some last examples, we focus on precipitates occurring in ternary Ni–Ti-based systems, such as Ni–Ti–Pd and Ni–Ti–Nb. For technical details on the sample preparation and used microscopy techniques, we refer to the respective papers.

Results and Discussion

Ni_5Al_3 in Ni–Al

For a long time, the Ni-rich part of the Ni–Al system, i.e. between 62 and 66 at.% Ni, was considered as a potential candidate for high-temperature SM behaviour since the transformation temperatures, although strongly depending on concentration, can go up to several hundreds of centigrades [2]. However, as is clear from the phase diagram originally published by Bradley and Taylor [3] and later refined by several others (see, e.g. [4]), when treating or operating the material at elevated temperatures up to 700 °C, the stable Ni_5Al_3 structure nucleates in the austenite B2 matrix and this new structure does not transform to martensite so no SM behaviour exists anymore. In fact, the basic lattice of this orthorhombic Ni_5Al_3 structure strongly resembles that of the tetragonal $L1_0$ martensite, the main difference being the accompanying diffusional component yielding a unit cell four times as large by doubling the shortest and one of the longest axes of the martensite cell and yielding twice as many variants [5, 6]. As a result, the nucleation of this structure is also accompanied by the formation of so-called self-accommodating structures in which the internal strain is minimised by the combination of several variants. In Fig. 1 an example of such a configuration is shown as observed at low magnification HRTEM in a $Ni_{62.5}Al_{27.5}$ sample annealed for 2 h at 550 °C and in which all three possible deformation variants are combined in two by two wings extending from a central nucleation point [5]. Despite the highly symmetric shape combining different variants and seen when observing the surrounding matrix along a $\langle 111 \rangle_{B2}$ direction, the accommodation is not perfect and the matrix-precipitate interfaces contain equidistant interfacial dislocations to accommodate the remaining interfacial lattice mismatch between the two structures. Assuming the Ni_5Al_3 structure has its expected stoichiometric concentration, which equals the nominal composition of the $Ni_{62.5}Al_{27.5}$ alloy, the nucleation and growth of these precipitates are only accompanied with local short range atom diffusion

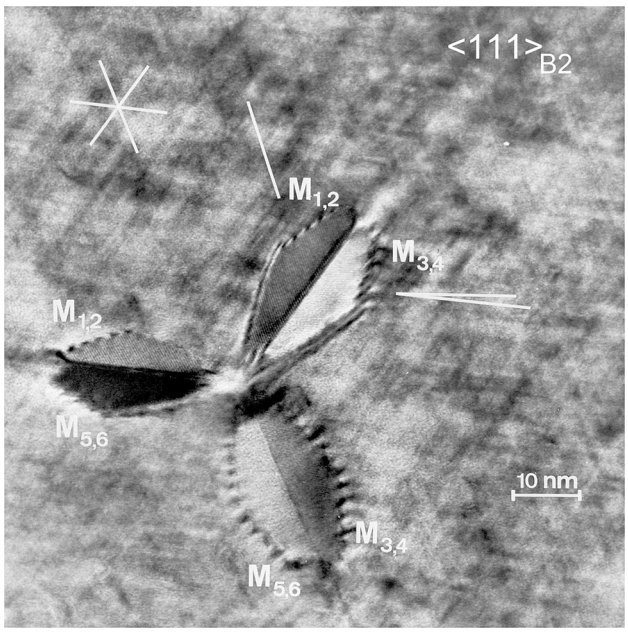

Fig. 1 $\langle 111 \rangle_{B2}$ low magnification HRTEM image of a star-shaped Ni_5Al_3 precipitate in annealed $Ni_{62.5}Al_{27.5}$ and combining different variants to minimise deformation strains. Still, interface dislocations are seen between the precipitate and matrix. (the indices refer to the two possibilities of ordering for each deformation variant) [6]

and will not influence the concentration of the surrounding matrix. As a result also the (low) transformation temperature and martensite 14M fine structure will be the same as for the original material [7]. Furthermore, according to the phase diagram, when continuing the annealing for longer times, the entire B2 austenite matrix will transform into this stable twinned Ni_5Al_3 structure and no martensitic transformation can be observed anymore. When annealing quenched material with slightly higher Ni concentrations, e.g. $Ni_{65}Al_{35}$, which is in the martensite state even at these elevated temperatures (e.g. 550 °C), the martensite lattice reorders directly into the Ni_5Al_3 structure, again stopping the possibility for any further displacive transformations [8]. In this particular system, the nucleation and growth of the ordered Ni_5Al_3 structure thus strongly hinder potential applications as SM or SE system, certainly at elevated temperatures.

Ni_4Ti_3 in Ni–Ti

In contrast to the disturbing effects of the nucleation and growth of the Ni_5Al_3 structure in Ni–Al, the Ni_4Ti_3 precipitates nucleating in near-equiatomic Ni-rich Ni–Ti material are very important for the martensitic transformation and related SM and SE effects [9]. Although these precipitates are metastable and will thus disappear after prolonged annealing times, controlled thermo-mechanical treatments can create particular configurations of lenticular

Ni_4Ti_3 precipitates in which the latter can act as nucleation sites of the transformation and support the SM behaviour at the microscopic level [10]. Moreover, due to the difference in concentration between the precipitates and the matrix and the resulting decrease of Ni in the latter upon precipitation, the annealing will stabilise the matrix concentration and thus the transformation temperatures, which are also in this system strongly dependent on composition [9, 11, 12].

Using the multislice least squares (MSLS) method, we first determined the exact atomic structure of well-developed Ni_4Ti_3 precipitates in a $Ni_{52}Ti_{48}$ alloy solution treated at 950 °C for 30 min followed by water quenching and ageing for 4 h at 520 °C [13]. In this method, electron diffraction intensities measured by a calibrated CCD are compared with simulated dynamical intensities calculated using the multislice method [14, 15]. By optimising the match between the experimental and calculated intensities, including the thickness and small misalignments as unknown parameters, site occupations and small atom shifts can be determined. As a result, the atomic positions of the Ni_4Ti_3 unit cell are refined, as shown in Fig. 2a, with no change in the R-3 symmetry of the earlier proposed unit cell [13]. The new unit cell also provides a better match between simulated and experimental high-resolution images, as seen in Fig. 2b. The observed atom shifts are found to be compatible with the lattice deformation by which the $\langle 111 \rangle_{B2}$ direction is compressed and the lens shaped precipitates are formed on $\{111\}_{B2}$ planes.

As a result of the collapse of one set of $\{111\}_{B2}$ planes upon formation of the Ni_4Ti_3 precipitates, a strain field develops surrounding the precipitate. Since the martensitic transformation upon cooling can nucleate at these precipitates, often in the form of the intermediate R-phase [10, 16], this strain field is of vital importance for the SM and SE behaviour. From single-conventional high-resolution TEM (HRTEM) images of small precipitates produced in a $Ni_{51}Ti_{49}$ alloy subjected to a heat treatment of 1 h at 950 °C followed by water quenching and subsequently aged for 4 h at 450 °C, the strain gradient in the surrounding matrix could be measured in 2D [17], while by combining two conventional HRTEM images obtained from different B2 zone axes, a 3D deformation matrix could be determined [18]. The symmetry and parameters of the latter correspond well with the transformation matrix of the R-phase, suggesting that this strain field indeed supports the R-phase nucleation at the precipitate-matrix interface. An example of a 2D strain map surrounding two nearby nanoprecipitates and obtained by geometric phase analysis (GPA) [19] from a HRTEM image is shown in Fig. 3a. At the same time, due to Ni enrichment in the precipitate, the surrounding matrix is depleted in Ni. This could be shown by spot-probe energy dispersive X-ray analysis (EDX) and electron energy loss spectroscopy

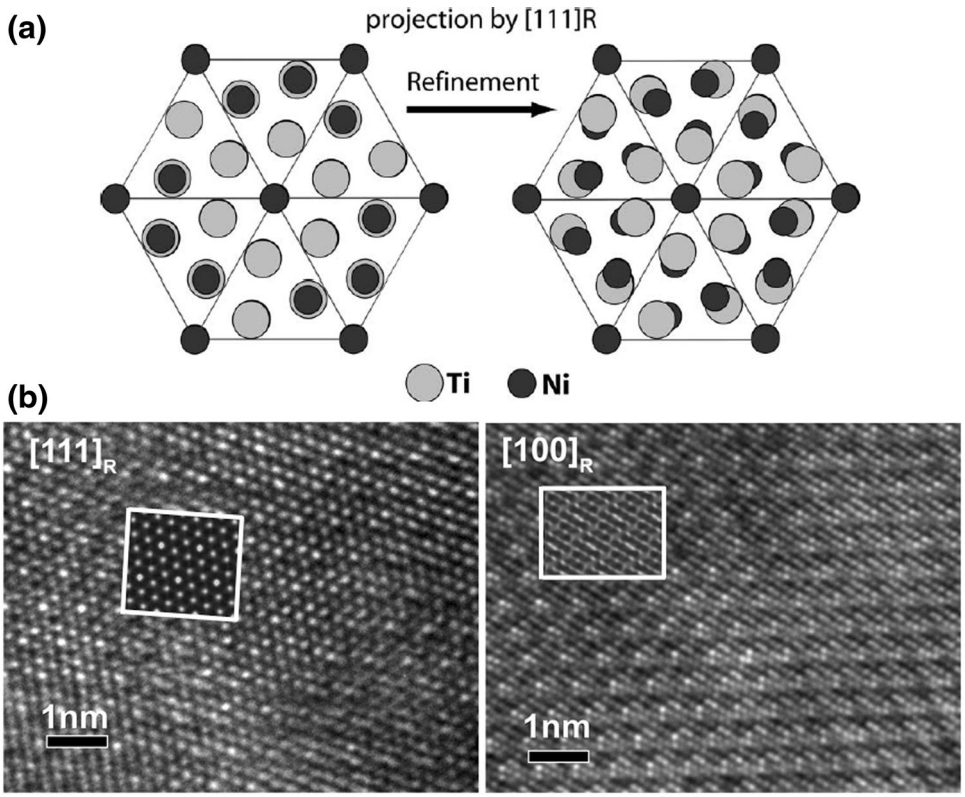

Fig. 2 **a** Ni_4Ti_3 unit cell as determined using MSLS optimisation and showing the atom shift when compared with the earlier model. **b** HRTEM images along two different zones including matching simulated *insets*. (the zones are defined in the rhombohedral (R) unit cell of the Ni_4Ti_3 structure) [13]

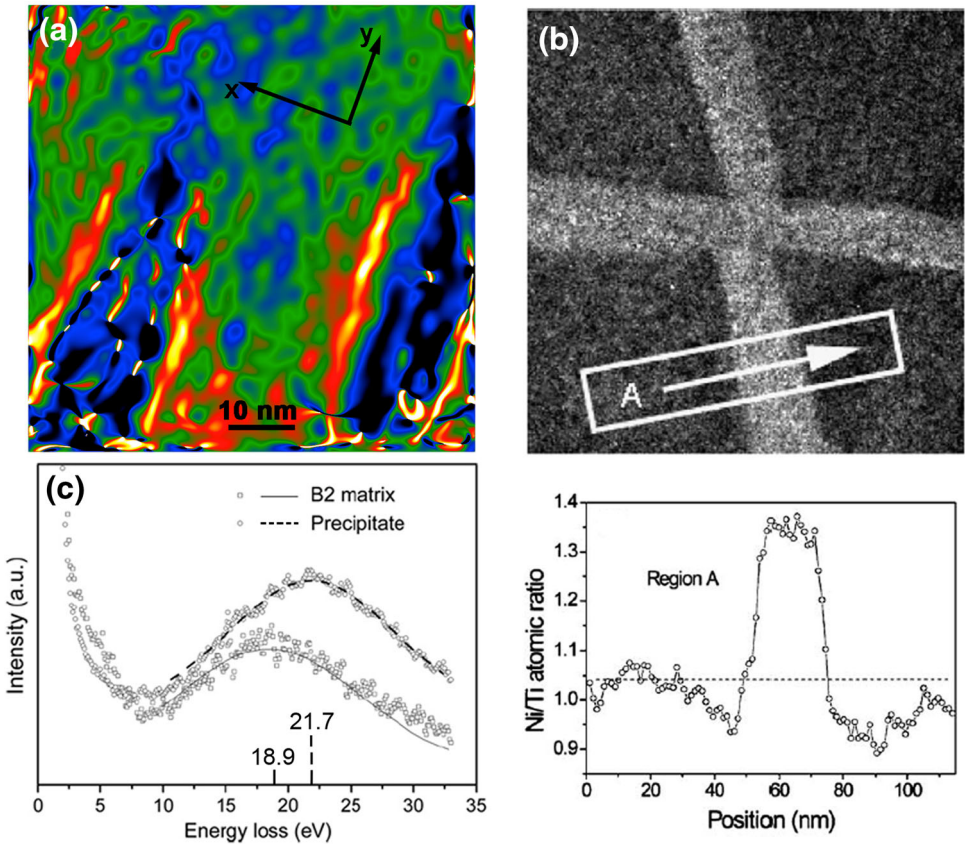

Fig. 3 **a** GPA map showing the strain gradients next to the long edges of Ni_4Ti_3 nanoprecipitates: the matrix is taken as a reference (*green*), the precipitates show a 1–2 % compression (*blue*), while the strongest relaxation (1–3 %) occurs alongside the long edges of the precipitates (*red* to *yellow*). **b** EDX Ni-map of two crossing precipitates with an averaged trace revealing Ni-depletion next to the precipitate. **c** EELS plasmon of the precipitate and austenite matrix [20, 22] (Color figure online)

(EELS) measurements, again in solution treated $Ni_{51}Ti_{49}$ but now annealed for 4 h at 500 °C, which revealed a small Ni-depleted region next to the precipitate and of approximately the same dimension as the latter [20] (Fig. 3b). Lowering the Ni content can also trigger the martensitic transformation, but recent results attribute a stronger effect to the strain field [21].

EELS was also used on the same sample to determine the elastic moduli of the metastable Ni_4Ti_3 precipitates, by measuring the plasmon energy and comparing this with the value for the matrix as reference as shown in Fig. 3c [22]. As a result, it was concluded that the precipitates have a Young's modulus of 163 ± 4 GPa, about 38 % higher than that of the matrix, in other words, the precipitates are harder than the matrix explaining why they are not deformed during the martensitic transformation of the austenite.

Although these intrinsic properties of a single Ni_4Ti_3 precipitate embedded in austenite B2 matrix are very relevant for understanding the transformation behaviour at the atomic scale, the macroscopic SM and SE behaviour will be more affected by the actual overall configuration and organisation of the Ni_4Ti_3 precipitates. For example, in polycrystalline samples, the heterogeneity of the nucleation and growth of Ni_4Ti_3 precipitates have been found to yielding various kinds of multistep transformations due to the existence of different areas of precipitates with various sizes and density [23–26]. Close to the grain boundary of grains of several microns in diameter, many small precipitates exist, while the interior of the grains exhibits none or fewer but larger precipitates, resulting in different transformation paths and Ms temperatures in those different regions. In order to quantify these microstructures in three dimensions, 3D slice-and-view was performed in a FIB/SEM yielding clear numerical differences between the various regions. In Fig. 4a the 3D configuration of the 4 families of micron-sized Ni_4Ti_3 precipitates observed in the centre of a large grain in a $Ni_{50.8}Ti_{49.2}$ alloy solution treated at 1000 °C for 1 h, water quenched and annealed for 1 h at 550 °C, is shown, while Fig. 4b shows the gradient from this region (right side) when moving closer to the grain boundary area (left side) with more but smaller precipitates [27, 28].

Moreover, when a material is annealed under stress, the Ni_4Ti_3 precipitates grow on preferential 111_{B2} planes so that ultimately only one family of precipitates will survive. In a single crystal sample of $Ni_{51}Ti_{49}$ annealed under $\langle 111 \rangle_{B2}$ stress (10 h, 550 °C, 50 MPa), the 3D investigation revealed box-like stackings of parallel precipitates as seen in Fig. 4c [29]. As a result, the martensite plates are

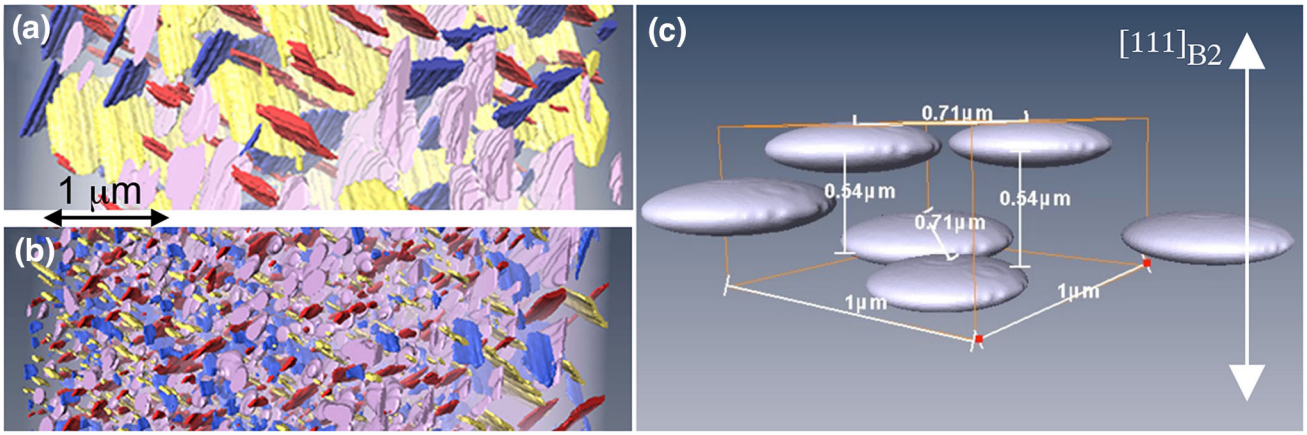

Fig. 4 3D configuration of Ni_4Ti_3 precipitates obtained by FIB/SEM slice-and-view in (**a**) the centre of a large grain and (**b**) closer towards the grain boundary (*left*). (**c**) The stacking of precipitates belonging to the same family as a result of annealing under stress along the indicated $[111]_{B2}$ direction [27, 29] (Color figure online)

strongly directed in between these parallel precipitates, although no long pathways exist, again affecting the macroscopic behaviour [16]. A similar phenomenon occurs in porous $Ni_{50.8}Ti_{49.2}$ material, aged for 6 h at 500 °C, where the stress field surrounding micron-sized pores can induce directional preference in the growth of the Ni_4Ti_3 precipitates, as seen in Fig. 5 [30].

Ni–Ti-X Ternary Systems

When binary Ni–Ti is alloyed with a third element, particular combinations of precipitates can occur depending on the solubility of the third element. For example, $Ni_{30}Ti_{50}Pd_{20}$ is investigated in the search for materials with low hysteresis and where the systematic replacement of Ni by Pd gradually changes the lattice parameters of the austenite and martensite so as to reach the $\lambda_2 = 1$ condition needed for minimal hysteresis [31]. In this system, several precipitation zones with different variants of tetragonal (C_{11b}) $Ti_2Pd(Ni)$ platelets in the austenite B2 matrix surrounding a single ellipsoid $Ti_2Ni(Pd)$ particle exhibiting a cubic (Fd3m) structure were observed (Fig. 6) [32]. Outside of this precipitation zone, the material is in its martensite B19 phase. It is assumed that during the annealing at 800 °C for 5.5 h and the following quench to room temperature local

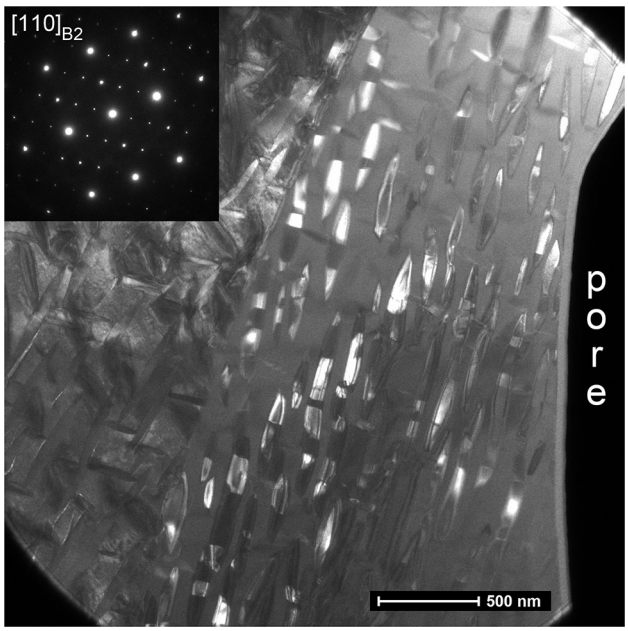

Fig. 5 Ni_4Ti_3 precipitates grown next to a pore in annealed porous $Ni_{50.8}Ti_{49.2}$. In the grain at the edge of the pore, the precipitates are aligned and belong nearly all to the same family, as also seen from the diffraction *inset*, while in the next grain (*left* side) precipitates of all variants have comparable sizes

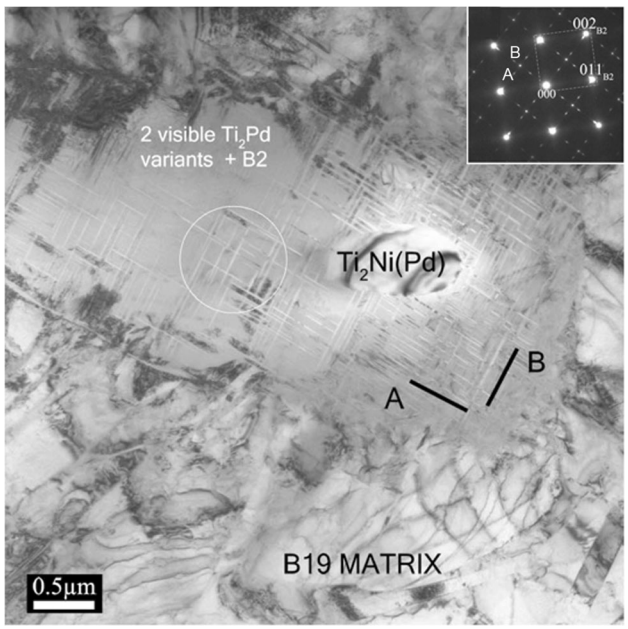

Fig. 6 Complex precipitation zone with different crystallographic variants of platelet Ti_2Pd precipitates surrounding an ellipsoid $Ti_2Ni(Pd)$ particle in homogenised $Ni_{30}Ti_{50}Pd_{20}$ [32]

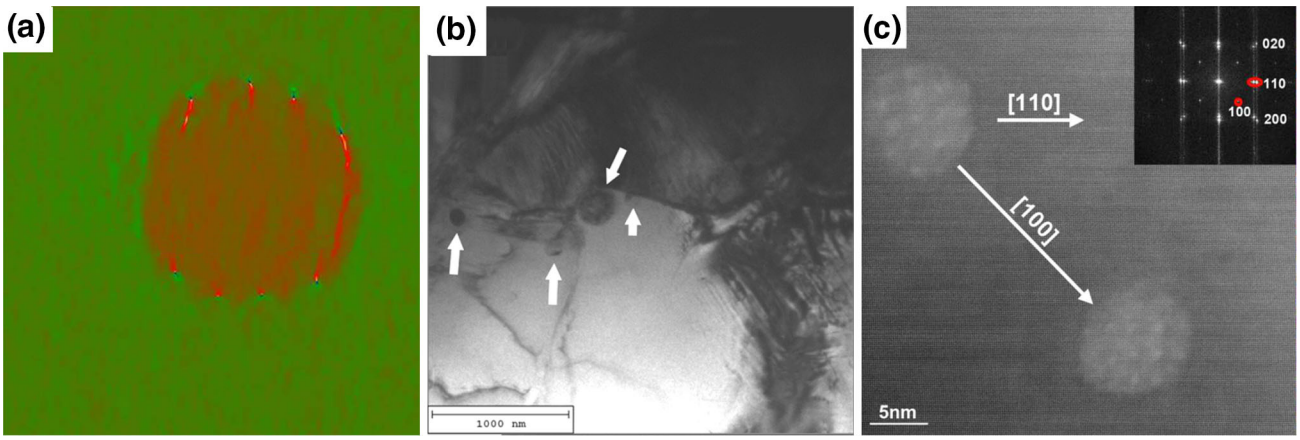

Fig. 7 **a** GPA of Nb-rich nano-sized precipitate in Ni–Ti–Nb revealing equidistant interface dislocations (as hotspots) accommodating the 10 % lattice mismatch between precipitate and matrix. **b** Austenite–martensite interface blocked by rows of nano-sized precipitates. **c** Two nanoprecipitates aligned along a cubic austenite direction [35, 36] (Color figure online)

fluctuations of the B2 matrix composition lead to the precipitation of $Ti_2Ni(Pd)$ particles accompanied by a precipitation of $Ti_2Pd(Ni)$ platelets in their immediate surroundings. Upon cooling, the B2 phase is retained in the immediate surroundings of the central $Ti_2Ni(Pd)$ precipitate since Ms is locally lowered due to a Pd depletion and/or a strengthening of the matrix by the coherent $Ti_2Pd(Ni)$ precipitates. Obviously, such local fluctuations and precipitation not only influence the local transformation but also hamper the search for the delicate balance between composition and lattice parameters.

On the other hand, in the Ni–Ti–Nb system, the third element is added to increase the hysteresis. In this case, the Nb has very low solubility in the Ni–Ti matrix and a eutectic structure with Nb-rich particles is formed. Still, some Nb is retained in the matrix and depending on the cooling or annealing conditions this Nb further precipitates into nanoparticles. Although there is a large lattice misfit of 10 % between the Nb-rich precipitates and the Ni–Ti matrix, both bcc-based structures, there is a one-to-one correlation between the respective lattice orientations with the lattice misfit being accommodated by interface dislocations every 10/11 {110} lattice planes of the precipitate and matrix, resp., as seen in Fig. 7a. This accommodation is very efficient so that only very little remaining strain inside the B2 matrix is observed. Although several investigations indicate that the response of the soft Nb-rich eutectic has the most pronounced effect on the transformation characteristics [33, 34], also these smaller precipitates can play an important role. Not only do they reduce the Nb content of the matrix, thus affecting the transformation temperatures via the concentration dependence [35], but they also hamper the movement of the transformation front as seen in the captured image of an in situ TEM annealing sequence where the austenite–martensite interface is seen to be halted by rows of precipitates formed in a commercial $(Ni–Ti)Nb_{8.4}$ alloy extruded and quenched from 900 °C (Fig. 7b) [36]. The latter already nucleate as aligned nanoscale precipitates along cubic directions of the austenite matrix in homogenised and quenched samples as seen in Fig. 7c.

Conclusions

In conclusion it can be stated that the formation of secondary phases by short or long-range diffusion, often as nano-sized precipitates, can have a profound effect on the shape memory and superelastic potential of a material undergoing a martensitic transformation. Depending on the case at hand, such secondary phases can decrease the probability of a displacive transformation by changing the phase stability in the system or can mechanically hinder the passage of the transformation interface. On the other hand, properly controlling the nucleation and growth of some precipitates can strongly improve the properties of some types of materials.

Acknowledgments The author gratefully thanks all researchers involved in the S/TEM investigations of the above listed examples: Y. Ma (NiAl), W. Tirry, Z.Q. Yang, S. Cao (NiTi), R. Delville (NiTiPd), H. Shi, (NiTiNb). The Flemish Science Foundation as well as the European Commission are acknowledged for financial support on various projects.

References

1. Cohen M, Olson GD, Clapp PC (1979) On the classification of displacive phase transformations. In: Proceedings of international conference on martensitic transformations ICOMAT-79 pp 1–6

2. Shapiro SM, Yang BX, Noda Y, Tanner LE, Schryvers D (1991) Neutron-scattering and electron-microscopy studies of the pre-martensitic phenomena in Ni_xAl_{100-x} alloys. Phys Rev B 44:9301–9313
3. Bradley AJ, Taylor A (1937) An X-ray analysis of the nickel–aluminium system. Proc R Soc Lond A 159:56–72
4. Okamoto H (2004) Al-Ni (Aluminum-Nickel). J Phase Equilib Diffus 25:394
5. Schryvers D, Ma Y, Toth L, Tanner L (1995) Electron microscopy study of the formation of Ni_5Al_3 in a $Ni_{62.5}Al_{37.5}$ B2 alloy I. Precipitation and growth. Acta Metall Mater 43:4045–4056
6. Schryvers D, Ma Y, Toth L, Tanner L (1995) Electron microscopy study of the formation of Ni_5Al_3 in a $Ni_{62.5}Al_{37.5}$ B2 alloy II. Plate crystallography. Acta Metall et Mater 43:4057–4065
7. Schryvers D (1993) Microtwin sequences in thermoelastic Ni_xAl_{100-x} martensite studied by conventional and high-resolution transmission electron microscopy. Philos Mag A 68:1017–1032
8. Schryvers D, Ma Y (1995) In situ TEM study of the Ni_5Al_3 to $B2 + L1_2$ decomposition in $Ni_{65}Al_{35}$. Mater Lett 23:105–111
9. Otsuka K, Ren X (2005) Physical metallurgy of Ti-Ni-based shape memory alloys. Prog Mater Sci 50:511–678
10. Bataillard L, Bidaux J-E, Gotthardt R (1998) Interaction between microstructure and multiple-step transformation in binary NiTi alloys using in situ transmission electron microscopy observations. Philos Mag A 78:327–344
11. Frenzel J, George EP, Dlouhy A, Somsen C, Wagner M-X, Eggeler G (2010) Influence of Ni on martensitic phase transformations in niti shape memory alloys. Acta Mater 58:3444–3458
12. Tang W (1997) Thermodynamic study of the low-temperature phase B19 and the martensitic transformation in near-equiatomic Ti-Ni shape memory alloys. Metall Mater Trans A 28:537–544
13. Tirry W, Schryvers D, Jorissen K, Lamoen D (2006) Electron-diffraction structure refinement of Ni_4Ti_3 precipitates in $Ni_{52}Ti_{48}$. Acta Crystallogr B 62:966–971
14. Jansen J, Tang D, Zandbergen HW, Schenk H (1998) MSLS, a least-squares procedure for accurate crystal structure refinement from dynamical electron diffraction patterns. Acta Crystallogr A 54:91–101
15. Jansen J, Zandbergen HW (2002) Determination of absolute configurations of crystal structures using electron diffraction patterns by means of least-squares refinement. Ultramicroscopy 90:291–300
16. Michutta J, Somsen C, Yawny A, Dlouhy A, Eggeler G (2006) Elementary martensitic transformation processes in Ni-rich NiTi single crystals with Ni_4Ti_3 precipitates. Acta Mater 54:3525–3542
17. Tirry W, Schryvers D (2005) Quantitative determination of strain fields around Ni_4Ti_3 precipitates in NiTi. Acta Mater 53:1041–1049
18. Tirry W, Schryvers D (2009) Linking a completely three-dimensional nanostrain to a structural transformation eigenstrain. Nat Mater 8:752–757
19. Hÿtch MJ, Snoeck E, Kilaas R (1998) Quantitative measurement of displacement and strain fields from HREM micrographs. Ultramicroscopy 74:131–146
20. Yang Z, Tirry W, Schryvers D (2005) Analytical TEM investigations on concentration gradients surrounding Ni_4Ti_3 precipitates in Ni-Ti shape memory material. Scr Mater 52:1129–1134
21. Wang X, Kustov S, Li K, Schryvers D, Verlinden B, Van Humbeeck J (2015) Effect of nanoprecipitates on the transformation behavior and functional properties of a Ti-50.8 at.% Ni alloy with micron-sized grains. Acta Mater 82:224–233
22. Yang Z, Tirry W, Lamoen D, Kulkova S, Schryvers D (2008) Electron energy-loss spectroscopy and first-principles calculation studies on a Ni-Ti shape memory alloy. Acta Mater 56:395–404
23. Khalil-Allafi J, Dlouhy J, Eggeler G (2002) Ni_4Ti_3-precipitation during aging of NiTi shape memory alloys and its influence on martensitic phase transformations. Acta Mater 50:4255–4274
24. Khalil-Allafi J, Ren X, Eggeler G (2002) The mechanism of multistage martensitic transformations in aged Ni-rich NiTi shape memory alloys. Acta Mater 50:793–803
25. Dlouhy A, Khalil-Allafi J, Eggeler G (2003) Multiple-step martensitic transformations in Ni-rich NiTi alloys—an in situ transmission electron microscopy investigation. Phil Mag 83:339–363
26. Nishida M, Hara T, Ohba T, Yamaguchi K, Tanaka K, Yamauchi K (2003) Experimental consideration of multistage martensitic transformation and precipitation behavior in aged Ni-rich Ti-Ni shape memory alloys. Mater Trans 44:2631–2636
27. Cao S, Nishida M, Schryvers D (2011) Quantitative three-dimensional analysis of Ni_4Ti_3 precipitate morphology and distribution in polycrystalline Ni-Ti. Acta Mater 59:1780–1789
28. Cao S, Pourbabak S, Schryvers D (2012) Quantitative 3-D morphologic and distributional study of Ni_4Ti_3 precipitates in a $Ni_{51}Ti_{49}$ single crystal alloy. Scr Mater 66:650–653
29. Cao S, Somsen C, Croitoru M, Schryvers D, Eggeler G (2010) Focused ion beam/scanning electron microscopy tomography and conventional transmission electron microscopy assessment of Ni_4Ti_3 morphology in compression-aged Ni-rich Ni-Ti single crystals. Scr Mater 62:399–402
30. Yao X, Cao S, Zhang XP, Schryvers D (2015) Microstructural characterization and transformation behavior of porous $Ni_{50.8}Ti_{49.2}$. Materials Today. In: Proceedings of international conference on martensitic transformations ICOMAT-2014 (to be published)
31. Cui J, Chu YS, Famodu OO, Furuya Y, Hattrick-Simpers J, James RD et al (2006) Combinatorial search of thermoelastic shape-memory alloys with extremely small hysteresis width. Nat Mater 5:286–290
32. Delville R, Schryvers D (2010) Transmission electron microscopy study of combined precipitation of $Ti_2Ni(Pd)$ and $Ti_2Pd(Ni)$ in a $Ti_{50}Ni_{30}Pd_{20}$ alloy. Intermetallics 18:2353–2360
33. Wang M, Jiang M, Liao G, Guo S, Zhao X (2012) Martensitic transformation involved mechanical behaviors and wide hysteresis of NiTiNb shape memory alloys. Prog Nat Sci 22:130–138
34. Zhao LC, Duerig TW, Justi S, Melton KN, Proft JL, Yu W, Wayman CM (1990) The study of Niobium-rich precipitates in a Ni-Ti-Nb shape memory alloy. Scr Metall Mater 24:221–225
35. Shi H, Frenzel J, Martinez GT, Van Rompaey S, Bakulin A, Kulkova S et al (2014) Site occupation of Nb atoms in ternary Ni-Ti-Nb shape memory alloys. Acta Mater 74:85–95
36. Shi H, Pourbabak S, Van Humbeeck J, Schryvers D (2012) Electron microscopy study of Nb-rich nanoprecipitates in Ni-Ti-Nb and their influence on the martensitic transformation. Scr Mater 67:939–942